Constraints on anomalous quartic gauge boson couplings from $\nu\bar{\nu}\gamma\gamma$ and $q\bar{q}\gamma\gamma$ events at CERN LEP2

G. Abbiendi,[2] C. Ainsley,[5] P. F. Åkesson,[3,v] G. Alexander,[21] J. Allison,[15] P. Amaral,[8] G. Anagnostou,[1] K. J. Anderson,[8] S. Asai,[22] D. Axen,[26] G. Azuelos,[17,a] I. Bailey,[25] E. Barberio,[7,n] T. Barillari,[31] R. J. Barlow,[15] R. J. Batley,[5] P. Bechtle,[24] T. Behnke,[24] K. W. Bell,[19] P. J. Bell,[1] G. Bella,[21] A. Bellerive,[6] G. Benelli,[4] S. Bethke,[31] O. Biebel,[30] O. Boeriu,[9] P. Bock,[10] M. Boutemeur,[30] S. Braibant,[7] L. Brigliadori,[2] R. M. Brown,[19] K. Buesser,[24] H. J. Burckhart,[7] S. Campana,[4] R. K. Carnegie,[6] A. A. Carter,[12] J. R. Carter,[5] C. Y. Chang,[16] D. G. Charlton,[1] C. Ciocca,[2] A. Csilling,[28] M. Cuffiani,[2] S. Dado,[20] A. De Roeck,[7] E. A. De Wolf,[7,q] K. Desch,[24] B. Dienes,[29] M. Donkers,[6] J. Dubbert,[30] E. Duchovni,[23] G. Duckeck,[30] I. P. Duerdoth,[15] E. Etzion,[21] F. Fabbri,[2] L. Feld,[9] P. Ferrari,[7] F. Fiedler,[30] I. Fleck,[9] M. Ford,[5] A. Frey,[7] P. Gagnon,[11] J. W. Gary,[4] G. Gaycken,[24] C. Geich-Gimbel,[3] G. Giacomelli,[2] P. Giacomelli,[2] M. Giunta,[4] J. Goldberg,[20] E. Gross,[23] J. Grunhaus,[21] M. Gruwé,[7] P. O. Günther,[3] A. Gupta,[8] C. Hajdu,[28] M. Hamann,[24] G. G. Hanson,[4] A. Harel,[20] M. Hauschild,[7] C. M. Hawkes,[1] R. Hawkings,[7] R. J. Hemingway,[6] G. Herten,[9] R. D. Heuer,[24] J. C. Hill,[5] K. Hoffman,[8] D. Horváth,[28,b] P. Igo-Kemenes,[10] K. Ishii,[22] H. Jeremie,[17] P. Jovanovic,[1] T. R. Junk,[6,g] N. Kanaya,[25] J. Kanzaki,[22,r] D. Karlen,[25] K. Kawagoe,[22] T. Kawamoto,[22] R. K. Keeler,[25] R. G. Kellogg,[16] B. W. Kennedy,[19] S. Kluth,[31] T. Kobayashi,[22] M. Kobel,[3] S. Komamiya,[22] T. Krämer,[24] P. Krieger,[6,j] J. von Krogh,[10] K. Kruger,[7] T. Kuhl,[24] M. Kupper,[23] G. D. Lafferty,[15] H. Landsman,[20] D. Lanske,[13] J. G. Layter,[4] D. Lellouch,[23] J. Letts,[m] L. Levinson,[23] J. Lillich,[9] S. L. Lloyd,[12] F. K. Loebinger,[15] J. Lu,[26,t] A. Ludwig,[3] J. Ludwig,[9] W. Mader,[3] S. Marcellini,[2] A. J. Martin,[12] G. Masetti,[2] T. Mashimo,[22] P. Mättig,[k] J. McKenna,[26] R. A. McPherson,[25] F. Meijers,[7] W. Menges,[24] F. S. Merritt,[8] H. Mes,[6,a] N. Meyer,[24] A. Michelini,[2] S. Mihara,[22] G. Mikenberg,[23] D. J. Miller,[14] S. Moed,[20] W. Mohr,[9] T. Mori,[22] A. Mutter,[9] K. Nagai,[12] I. Nakamura,[22,s] H. Nanjo,[22] H. A. Neal,[32] R. Nisius,[31] S. W. O'Neale,[1] A. Oh,[7] M. J. Oreglia,[8] S. Orito,[22,x] C. Pahl,[31] G. Pásztor,[4,e] J. R. Pater,[15] J. E. Pilcher,[8] J. Pinfold,[27] D. E. Plane,[7] B. Poli,[2] O. Pooth,[13] M. Przybycień,[7,l] A. Quadt,[3] K. Rabbertz,[7,p] C. Rembser,[7] P. Renkel,[23] J. M. Roney,[25] Y. Rozen,[20] K. Runge,[9] K. Sachs,[6] T. Saeki,[22] E. K. G. Sarkisyan,[7,h] A. D. Schaile,[30] O. Schaile,[30] P. Scharff-Hansen,[7] J. Schieck,[31] T. Schörner-Sadenius,[7,w] M. Schröder,[7] M. Schumacher,[3] W. G. Scott,[19] R. Seuster,[13,d] T. G. Shears,[7,f] B.C. Shen,[4] P. Sherwood,[14] A. Skuja,[16] A. M. Smith,[7] R. Sobie,[25] S. Söldner-Rembold,[14] F. Spano,[8] A. Stahl,[3,u] D. Strom,[18] R. Ströhmer,[30] S. Tarem,[20] M. Tasevsky,[7,q] R. Teuscher,[8] M. A. Thomson,[5] E. Torrence,[18] D. Toya,[22] P. Tran,[4] I. Trigger,[7] Z. Trócsányi,[29,c] E. Tsur,[21] M. F. Turner-Watson,[1] I. Ueda,[22] B. Ujvári,[29,c] C. F. Vollmer,[30] P. Vannerem,[9] R. Vértesi,[29,c] M. Verzocchi,[16] H. Voss,[7,o] J. Vossebeld,[7,f] C. P. Ward,[5] D. R. Ward,[5] P. M. Watkins,[1] A. T. Watson,[1] N. K. Watson,[1] P. S. Wells,[7] T. Wengler,[7] N. Wermes,[3] G. W. Wilson,[15,i] J. A. Wilson,[1] G. Wolf,[23] T. R. Wyatt,[15] S. Yamashita,[22] D. Zer-Zion,[4] and L. Zivkovic[23]

(OPAL Collaboration)

[1]*School of Physics and Astronomy, University of Birmingham, Birmingham B15 2TT, United Kingdom*
[2]*Dipartimento di Fisica dell' Università di Bologna and INFN, I-40126 Bologna, Italy*
[3]*Physikalisches Institut, Universität Bonn, D-53115 Bonn, Germany*
[4]*Department of Physics, University of California, Riverside, California 92521, USA*
[5]*Cavendish Laboratory, Cambridge CB3 0HE, United Kingdom*
[6]*Ottawa-Carleton Institute for Physics, Department of Physics, Carleton University, Ottawa, Ontario, Canada K1S 5B6*
[7]*CERN, European Organisation for Nuclear Research, CH-1211 Geneva 23, Switzerland*
[8]*Enrico Fermi Institute and Department of Physics, University of Chicago, Chicago, Illinois 60637, USA*
[9]*Fakultät für Physik, Albert-Ludwigs-Universität Freiburg, D-79104 Freiburg, Germany*
[10]*Physikalisches Institut, Universität Heidelberg, D-69120 Heidelberg, Germany*
[11]*Department of Physics, Indiana University, Bloomington, Indiana 47405, USA*
[12]*Queen Mary and Westfield College, University of London, London E1 4NS, United Kingdom*
[13]*Technische Hochschule Aachen, III Physikalisches Institut, Sommerfeldstrasse 26-28, D-52056 Aachen, Germany*
[14]*University College London, London WC1E 6BT, United Kingdom*
[15]*Department of Physics, Schuster Laboratory, The University, Manchester M13 9PL, United Kingdom*
[16]*Department of Physics, University of Maryland, College Park, Maryland 20742, USA*
[17]*Laboratoire de Physique Nucléaire, Université de Montréal, Montréal, Québec, Canada H3C 3J7*
[18]*University of Oregon, Department of Physics, Eugene, Oregon 97403, USA*
[19]*CCLRC Rutherford Appleton Laboratory, Chilton, Didcot, Oxfordshire OX11 0QX, United Kingdom*
[20]*Department of Physics, Technion-Israel Institute of Technology, Haifa 32000, Israel*
[21]*Department of Physics and Astronomy, Tel Aviv University, Tel Aviv 69978, Israel*
[22]*International Centre for Elementary Particle Physics and Department of Physics, University of Tokyo, Tokyo 113-0033, Japan and Kobe University, Kobe 657-8501, Japan*
[23]*Particle Physics Department, Weizmann Institute of Science, Rehovot 76100, Israel*
[24]*Universität Hamburg/DESY, Institut für Experimentalphysik, Notkestrasse 85, D-22607 Hamburg, Germany*
[25]*University of Victoria, Department of Physics, P O Box 3055, Victoria BC, Canada V8W 3P6*

[26]*University of British Columbia, Department of Physics, Vancouver BC, Canada V6T 1Z1*
[27]*University of Alberta, Department of Physics, Edmonton AB, Canada T6G 2J1*
[28]*Research Institute for Particle and Nuclear Physics, H-1525 Budapest, P O Box 49, Hungary*
[29]*Institute of Nuclear Research, H-4001 Debrecen, P O Box 51, Hungary*
[30]*Ludwig-Maximilians-Universität München, Sektion Physik, Am Coulombwall 1, D-85748 Garching, Germany*
[31]*Max-Planck-Institute für Physik, Föhringer Ring 6, D-80805 München, Germany*
[32]*Yale University, Department of Physics, New Haven, Connecticut 06520, USA*
(Received 23 February 2004; published 27 August 2004)

Anomalous quartic couplings between the electroweak gauge bosons may contribute to the $\nu\bar{\nu}\gamma\gamma$ and $q\bar{q}\gamma\gamma$ final states produced in e^+e^- collisions. This analysis uses the LEP2 OPAL data sample at center-of-mass energies up to 209 GeV. Event selections identify $\nu\bar{\nu}\gamma\gamma$ and $q\bar{q}\gamma\gamma$ events in which the two photons are reconstructed within the detector acceptance. The cross section for the process $e^+e^-\to q\bar{q}\gamma\gamma$ is measured. Averaging over all energies, the ratio of the observed $e^+e^-\to q\bar{q}\gamma\gamma$ cross section to the standard model expectation is $R(\text{data/SM})=0.92\pm0.07\pm0.04$, where the errors represent the statistical and systematic uncertainties respectively. The $\nu\bar{\nu}\gamma\gamma$ and $q\bar{q}\gamma\gamma$ data are used to constrain possible anomalous $W^+W^-\gamma\gamma$ and $ZZ\gamma\gamma$ couplings. Combining with previous OPAL results from the $W^+W^-\gamma$ final state, the 95% confidence level limits on the anomalous coupling parameters a_0^Z, a_c^Z, a_0^W and a_c^W are found to be $-0.007\ \text{GeV}^{-2}<a_0^Z/\Lambda^2<0.023\ \text{GeV}^{-2}$, $-0.029\ \text{GeV}^{-2}<a_c^Z/\Lambda^2<0.029\ \text{GeV}^{-2}$, $-0.020\ \text{GeV}^{-2}<a_0^W/\Lambda^2<0.020\ \text{GeV}^{-2}$, $-0.052\ \text{GeV}^{-2}<a_c^W/\Lambda^2<0.037\ \text{GeV}^{-2}$, where Λ is the energy scale of the new physics. Limits found when allowing two or more parameters to vary are also presented.

DOI: 10.1103/PhysRevD.70.032005 PACS number(s): 13.66.Fg

I. INTRODUCTION

In the standard model (SM) self-interactions of the vector boson fields arise due to the $-\frac{1}{4}\mathbf{W_{\mu\nu}}\cdot\mathbf{W^{\mu\nu}}$ term in the electroweak Lagrangian. In addition to the tri-linear couplings, this term leads to quartic gauge couplings (QGCs) of the form WWWW, WWZZ, WW$\gamma\gamma$ and WWZγ. The strength of the coupling at these vertices is specified by the SU(2) $\times$U(1) gauge invariant form of the electroweak sector. Studying processes to which these QGCs can contribute may therefore yield further confirmation of the non-Abelian structure of the SM or signal the presence of new physics at as yet unprobed energy scales. At LEP energies it is only possible to probe quartic gauge couplings which produce at most two massive vector bosons in the final state. The processes at LEP which are sensitive to possible anomalous quartic gauge couplings (AQGCs) are shown in Fig. 1.

The formalism for the extra genuine quartic terms relevant at LEP has been discussed widely in the literature [1–7]. Genuine quartic terms refer to those that are not associated with any tri-linear couplings, which are already constrained by analyses using the $e^+e^-\to W^+W^-$ process. In the parametrization first introduced in [1] the two lowest dimension terms that give rise to quartic couplings involving at least two photons are:

[a]Also at TRIUMF, Vancouver, Canada V6T 2A3.
[b]Also at Institute of Nuclear Research, Debrecen, Hungary.
[c]Also at Department of Experimental Physics, University of Debrecen, Hungary.
[d]Also at MPI München, Germany.
[e]Also at Research Institute for Particle and Nuclear Physics, Budapest, Hungary.
[f]Now at University of Liverpool, Dept. of Physics, Liverpool L69 3BX, U.K.
[g]Now at Dept. Physics, University of Illinois at Urbana-Champaign, Urbana-Champaign, IL, U.S.A.
[h]Also at Manchester University, Manchester M13 9PL U.K.
[i]Now at University of Kansas, Dept. of Physics and Astronomy, Lawrence, KS 66045, U.S.A.
[j]Now at University of Toronto, Dept. of Physics, Toronto, Canada.
[k]Current address: Bergische Universität, Wuppertal, Germany.
[l]Now at University of Mining and Metallurgy, Cracow, Poland.
[m]Now at University of California, San Diego, CA, U.S.A.
[n]Now at The University of Melbourne, Victoria, Australia.
[o]Now at IPHE Université de Lausanne, CH-1015 Lausanne, Switzerland.
[p]Now at IEKP Universität Karlsruhe, Germany.
[q]Now at University of Antwerpen, Physics Department, B-2610 Antwerpen, Belgium.
[r]Also at High Energy Accelerator Research Organisation (KEK), Tsukuba, Ibaraki, Japan.
[s]Now at University of Pennsylvania, Philadelphia, Pennsylvania, USA.
[t]Now at TRIUMF, Vancouver, Canada.
[u]Now at DESY Zeuthen, D-15788 Zeuthen, Germany.
[v]Now at CERN, CH-1211 Geneva 23, Switzerland.
[w]Now at DESY, D-22607, Hamburg, Germany.
[x]Deceased.

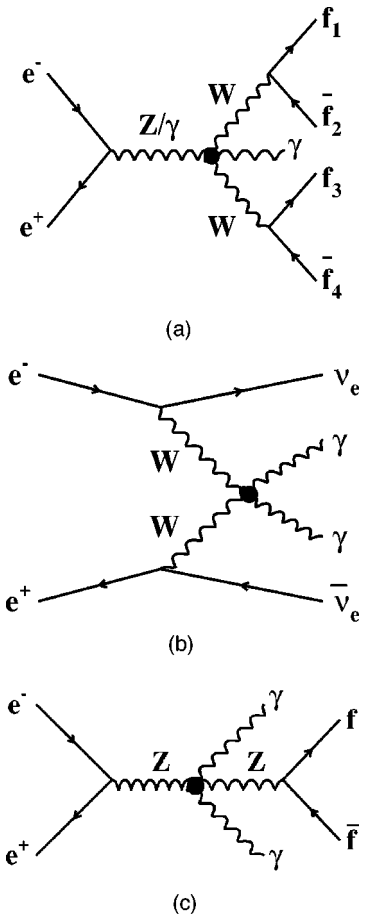

FIG. 1. The diagrams sensitive to possible anomalous quartic couplings in the $e^+e^-\to \mathrm{W}^+\mathrm{W}^-\gamma$, $e^+e^-\to\nu\bar{\nu}\gamma\gamma$ and $e^+e^-\to q\bar{q}\gamma\gamma$ final states.

$$\mathcal{L}_6^0 = -\frac{e^2}{16}\frac{a_0}{\Lambda^2}F_{\mu\nu}F^{\mu\nu}\vec{W}^\alpha\cdot\vec{W}_\alpha,$$

$$\mathcal{L}_6^c = -\frac{e^2}{16}\frac{a_c}{\Lambda^2}F_{\mu\alpha}F^{\mu\beta}\vec{W}^\alpha\cdot\vec{W}_\beta,$$

where $F^{\mu\nu}$ is the photon field strength tensor. These are C and P conserving and are obtained by imposing local $\mathrm{U}(1)_{\mathrm{em}}$ gauge symmetry, whilst also requiring the global custodial $\mathrm{SU}(2)_c$ symmetry that preserves the constraint that the electroweak parameter $\rho=1$. We note that the custodial $\mathrm{SU}(2)_c$ field vector is

$$\vec{W}_\alpha = \begin{pmatrix} \frac{1}{\sqrt{2}}(W_\alpha^+ + W_\alpha^-) \\ \frac{i}{\sqrt{2}}(W_\alpha^+ - W_\alpha^-) \\ Z_\alpha/\cos\theta_W \end{pmatrix}$$

and identifying

$$\vec{W}_\alpha\cdot\vec{W}_\beta \to 2\left(W_\alpha^+W_\beta^- + \frac{1}{2\cos^2\theta_W}Z_\alpha Z_\beta\right)$$

yields, in terms of the physical fields, W_α^+, W_α^- and Z_α,

$$\mathcal{L}_6^0 = -\frac{e^2}{8}\frac{a_0^{\mathrm{W}}}{\Lambda^2}F_{\mu\nu}F^{\mu\nu}W^{+\alpha}W_\alpha^- - \frac{e^2}{16\cos^2\theta_W}\frac{a_0^{\mathrm{Z}}}{\Lambda^2}F_{\mu\nu}F^{\mu\nu}Z^\alpha Z_\alpha,$$

$$\mathcal{L}_6^c = -\frac{e^2}{16}\frac{a_c^{\mathrm{W}}}{\Lambda^2}F_{\mu\alpha}F^{\mu\beta}(W^{+\alpha}W_\beta^- + W^{-\alpha}W_\beta^+) - \frac{e^2}{16\cos^2\theta_W}\frac{a_c^{\mathrm{Z}}}{\Lambda^2}F_{\mu\alpha}F^{\mu\beta}Z^\alpha Z_\beta.$$

Thus, both $\mathcal{L}_6^0$ and $\mathcal{L}_6^c$ generate $\mathrm{W}^+\mathrm{W}^-\gamma\gamma$ and $\mathrm{ZZ}\gamma\gamma$ couplings, with the parameters a_0 and a_c now being distinguished for the W and Z vertices to comply with the more general treatment in [5]. In all cases the strengths of the quartic couplings are proportional to $1/\Lambda^2$ where Λ is interpreted as the energy scale of the new physics.

Limits on AQGCs from LEP data have been published by the OPAL and L3 Collaborations [8–11]. This paper describes limits on AQGCs obtained by OPAL from the processes $e^+e^-\to\nu\bar{\nu}\gamma\gamma$ and $e^+e^-\to q\bar{q}\gamma\gamma$ from all data recorded above the Z pole. For both processes the dominant SM background arises from initial-state radiation (ISR). The limits obtained from $e^+e^-\to\nu\bar{\nu}\gamma\gamma$ and $e^+e^-\to q\bar{q}\gamma\gamma$ are combined with the limits obtained by OPAL from the process $e^+e^-\to\mathrm{W}^+\mathrm{W}^-\gamma$ [11].

Since cross sections for the $q\bar{q}\gamma\gamma$ final state have not previously been measured explicitly by the OPAL Collaboration at LEP2, these measurements are presented in this paper and are compared with the SM expectation.

II. THE OPAL DETECTOR AND DATA SAMPLES

The OPAL detector included a 3.7 m diameter tracking volume within a 0.435 T axial magnetic field. The tracking detectors included a silicon micro-vertex detector, a high precision gas vertex detector and a large volume gas jet chamber. The tracking acceptance corresponds to approximately

$|\cos\theta|<0.95$ (for the track quality cuts used in this study).[1] Lying outside the solenoid, the electromagnetic calorimeter (ECAL) consisted of 11 704 lead glass blocks having full acceptance in the range $|\cos\theta|<0.98$ and a relative energy resolution of approximately 6% for 10 GeV photons. The hadron calorimeter consisted of the magnet return yoke instrumented with streamer tubes. Muon chambers outside the hadronic calorimeter provided muon identification in the range $|\cos\theta|<0.98$. A detailed description of the OPAL detector can be found in [12].

From 1995 to 2000 the LEP center-of-mass energy was increased in several steps from 130 to 209 GeV. For the analysis of the $q\bar{q}\gamma\gamma$ channel, this entire data sample is used, corresponding to 712 pb^{-1}. The $\nu\bar{\nu}\gamma\gamma$ analysis is restricted to 652 pb^{-1} of data recorded above 180 GeV. The integrated luminosities at each center-of-mass energy for the $\nu\bar{\nu}\gamma\gamma$ analysis are lower than those for the $q\bar{q}\gamma\gamma$ analysis due to tighter requirements on the operational status of the detector components.

III. MONTE CARLO MODELS

A number of Monte Carlo (MC) samples, all including a full simulation [13] of the OPAL detector, are used to simulate the SM signal and background processes. For the $\nu\bar{\nu}\gamma\gamma$ final state NUNUGPV [14] is used to model both the dominant SM doubly-radiative return process and the supplementary AQGC processes, with KK2F [15] being used as a cross-check on the SM expectations. For the $q\bar{q}\gamma\gamma$ final state, the KK2F program is also used. For the background processes, the concurrent MC tandem [16] of KORALW and YFSWW is used to simulate the background from four-fermion final states with fermion flavor consistent with being from $\mathrm{W}^+\mathrm{W}^-$ final states. The KORALW program [17] is used to simulate the background from four-fermion final states which are incompatible with coming from the decays of two W-bosons (e.g. $e^+e^-\to q\bar{q}\mu^+\mu^-$). For both signal and background processes JETSET [18] is used to model the fragmentation and hadronisation of final state quarks. The two-fermion background process $e^+e^-\to \mathrm{Z}/\gamma\to\tau^+\tau^-$ is simulated using KK2F. The background in the $q\bar{q}\gamma\gamma$ event selection from multi-peripheral two-photon diagrams is negligible. The WRAP program [7] is used to determine the effects of AQGCs in the $q\bar{q}\gamma\gamma$ channel.

IV. THE $\nu\bar{\nu}\gamma\gamma$ FINAL STATE

A. $\nu\bar{\nu}\gamma\gamma$ event selection

The selection proceeds in two stages:

Acoplanar photon pair selection: This event selection employs standard criteria described in detail elsewhere [19,20]. Candidate events must meet the kinematic requirement of there being at least two photons, either both with energy $E_\gamma>0.05E_{\mathrm{beam}}$ and polar angle θ_γ satisfying $|\cos\theta_\gamma|<0.966$, or one with $E_\gamma>0.05E_{\mathrm{beam}}$, $|\cos\theta_\gamma|<0.966$ accompanied by a second with $E_\gamma>1.75$ GeV, $|\cos\theta_\gamma|<0.8$ that has an associated in-time time-of-flight detector signal. Events with three final state photons ($e^+e^-\to\nu\bar{\nu}\gamma\gamma\gamma$) are permitted, the subsequent selection criteria then being applied to the two photons with the highest reconstructed energies. The system consisting of the two highest energy photons must have a momentum transverse to the beam axis, $p_T^{\gamma\gamma}$, satisfying $p_T^{\gamma\gamma}>0.05E_{\mathrm{beam}}$. Additional requirements are then made on the photon conversion consistency (charged track veto), the electromagnetic calorimeter cluster shape, the forward energy vetoes and the muon vetoes. The $e^+e^-\to\gamma\gamma(\gamma)$ background is suppressed whilst retaining the events with missing energy by imposing further cuts on the energies and angles of the selected two or three photon system. These include the requirements that the total energy in the electromagnetic calorimeter does not exceed $0.95\sqrt{s}$ and also that the acoplanarity[2] angle of the two highest energy photons be greater than 2.5°.

The efficiency for SM $e^+e^-\to\nu\bar{\nu}\gamma\gamma(\gamma)$ events within the kinematic acceptance of the acoplanar photon pair selection is approximately 66% [20]. The expected background contribution from processes other than $e^+e^-\to\nu\bar{\nu}\gamma\gamma(\gamma)$ is less than 1% [19,20].

Suppression of standard model background: To suppress the SM contribution, principally the forward-peaked doubly-radiative return process, the following additional cuts are applied to the events passing the acoplanar photon pair selection:

The two highest reconstructed photon energies, $E_{\gamma 1}$ and $E_{\gamma 2}$, must both be greater than 10 GeV. This cut has little effect on any AQGC contribution, which gives rise predominantly to photons of high energy, but does suppress the doubly-radiative return background.

$|\cos\theta_{\gamma 1}|<0.9$, $|\cos\theta_{\gamma 2}|<0.9$, where again the subscripts refer to the two photons with highest reconstructed energy. This requirement further suppresses the doubly-radiative return background, which is forward peaked as expected for initial-state radiation photons.

These cuts were optimized on SM MC to yield the maximum sensitivity to the anomalous couplings.

B. Sensitivity of $e^+e^-\to\nu\bar{\nu}\gamma\gamma$ to anomalous QGCs

Table I lists the number of data events accepted by the $\nu\bar{\nu}\gamma\gamma$ event selection compared to the SM expectation, binned by center-of-mass energy. There is excellent agreement between the predictions of NUNUGPV and the KK2F MC program [15] used as a cross-check. The SM predictions describe the data well.

[1]The OPAL right-handed coordinate system is defined such that the origin is at the center of the detector and the z axis points along the direction of the e^- beam; θ is the polar angle with respect to the z axis.

[2]The acoplanarity angle is defined as π minus the opening angle between the two photons when projected onto a plane perpendicular to the beam axis.

TABLE I. Numbers of $\nu\bar{\nu}\gamma\gamma$ events passing the event selection by center-of-mass energy compared to the SM expectations from both KK2F and NUNUGPV. All MC accepted cross sections have been corrected for efficiency losses due to random coincident detector hits.

$\sqrt{s}$ (GeV)	$\int \mathcal{L}dt$ (pb^{-1})	Data	SM expectation	
			NUNUGPV	KK2F
180–185	53.9	0	2.5	2.5
188–190	175.2	10	7.9	7.9
191–192	28.8	1	1.3	1.3
195–196	71.6	0	3.1	3.0
199–201	73.7	3	3.0	2.9
201–203	36.7	1	1.5	1.4
203–209	210.6	5	8.3	8.0
Total	652	20	27.6	27.0

Approximately 4.0–4.7 % of real data events, depending on the center-of-mass energy, are expected to fail the acoplanar selection due to the effects of random coincidental activity. These rates have been evaluated from samples of random beam-crossing events collected throughout the data-taking periods. All quoted MC accepted cross sections have been corrected for these unmodelled effects.

For the selected events, Fig. 2 shows the distribution of the invariant mass recoiling against the photons, M_{rec}, and the distribution of the energy of the photon with the second highest reconstructed energy, $E_{\gamma 2}$. In both cases the data are well described by the SM expectation. Figure 2 also shows the effects of anomalous couplings on these distributions. For the recoil mass, increasing the coupling at the $\mathrm{ZZ}\gamma\gamma$ vertex increases the cross section at the Z mass peak, whereas the effect of the $\mathrm{W^+W^-}\gamma\gamma$ vertex can mainly be seen in the low recoil mass region of the plot. Similarly, the effects of the different quartic vertices can be distinguished in different regions of the $E_{\gamma 2}$ distribution.

Constraints on AQGCs are derived employing a maximum likelihood fit that uses bins in the M_{rec} and $E_{\gamma 2}$ distributions at each center-of-mass energy. The ten bins are defined in Table II, together with the corresponding numbers of events observed and expected in the SM summed over center-of-mass energies. The choice of binning reflects the

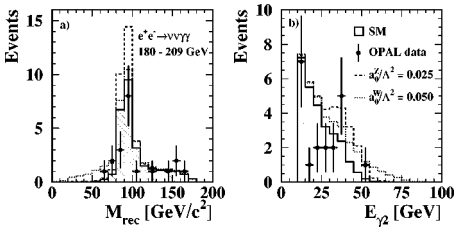

FIG. 2. Distributions of (a) M_{rec} and (b) $E_{\gamma 2}$ for the accepted $\nu\bar{\nu}\gamma\gamma$ events. The points show the 180–209 GeV data and the histograms show the MC expectation. The hatched histogram represents the SM scenario whilst the expected distributions for possible $\mathrm{ZZ}\gamma\gamma$ and $\mathrm{W^+W^-}\gamma\gamma$ AQGC hypotheses are shown by the dashed and dotted lines, respectively.

TABLE II. The binning of the likelihood function for the $\nu\bar{\nu}\gamma\gamma$ events together with the corresponding numbers of events observed and expected in the SM.

Bin number	M_{rec} (GeV)	$E_{\gamma 2}$ (GeV)	Observed	Expected
1	<60	10–25	0	0.1
2	<60	25–45	0	<0.1
3	<60	>45	0	<0.1
4	60–80	10–25	1	0.5
5	60–80	25–45	2	0.4
6	60–80	>45	0	0.1
7	80–120	10–25	5	11.7
8	80–120	25–45	6	8.3
9	80–120	>45	1	0.8
10	>120	>10	5	5.7
	Total		20	27.6

differing effects of the anomalous couplings on the different regions of the M_{rec} and $E_{\gamma 2}$ distributions and was optimized on SM MC for maximum sensitivity to the coupling parameters, inclusive of systematic effects.

Systematic uncertainties ($\nu\bar{\nu}\gamma\gamma$)

The systematic errors in this analysis are found to be small in comparison to the statistical error from the 20 selected data events.

Experimental uncertainties: The main experimental systematic uncertainty arises from the accuracy of the modeling of the energy scale and resolution of the electromagnetic calorimeter. The evaluation of this is based on a comparison of reconstructed events with two beam-energy photons in the final state $e^+e^-\to\gamma\gamma$ with those simulated in MC. Additional degradations in the resolution and scaling were then applied to the accepted SM cross sections (both total and in the analysis bins) to evaluate the systematic uncertainties, separately for the barrel ($|\cos\theta_\gamma|<0.7$) and end-cap ($0.7<|\cos\theta_\gamma|<0.9$) regions of the detector and for each year of data taking. These uncertainties result in relatively large fractional systematic uncertainties for individual analysis bins (approximately 20% for the bins with smallest cross section, i.e. bins 2 and 3 of Table II) though these propagate through to small overall errors of less than 1% on the total cross sections. Possible biases in the measured photon angle were found to be negligible.

Theory shape uncertainty: The shapes of the SM M_{rec} and $E_{\gamma 2}$ distributions from KK2F and NUNUGPV have been compared in order to evaluate any possible theoretical uncertainty in the SM prediction. Again, the variations in the total cross sections were small ($<4\%$), but large fractional variations could be seen for bins 1–3 which were hardly populated by the statistics available from KK2F.

Normalization uncertainty: Other sources of systematic uncertainty have been considered and affect primarily the overall normalization. The uncertainty related to the modeling of initial-state radiation (ISR) has been assessed by turning off ISR with finite p_T, leading to a $\pm 5\%$ normalization

TABLE III. The 95% C.L. limits on the anomalous QGCs from the OPAL LEP2 data from the processes shown in Fig. 1. The $\nu\bar{\nu}\gamma\gamma$ and $q\bar{q}\gamma\gamma$ results are described in this paper. The limits from the process $e^+e^-\to W^+W^-\gamma$ are described in Ref. [11]. All limits include systematic uncertainties and correspond to the case where only the coupling in question is varied from zero.

Process	Coupling	95% C.L. Limit
$\nu\bar{\nu}\gamma\gamma$	a_0^Z	$-0.009\ \text{GeV}^{-2}<a_0^Z/\Lambda^2<0.026\ \text{GeV}^{-2}$
$\nu\bar{\nu}\gamma\gamma$	a_c^Z	$-0.034\ \text{GeV}^{-2}<a_c^Z/\Lambda^2<0.039\ \text{GeV}^{-2}$
$\nu\bar{\nu}\gamma\gamma$	a_0^W	$-0.040\ \text{GeV}^{-2}<a_0^W/\Lambda^2<0.037\ \text{GeV}^{-2}$
$\nu\bar{\nu}\gamma\gamma$	a_c^W	$-0.114\ \text{GeV}^{-2}<a_c^W/\Lambda^2<0.103\ \text{GeV}^{-2}$
$q\bar{q}\gamma\gamma$	a_0^Z	$-0.012\ \text{GeV}^{-2}<a_0^Z/\Lambda^2<0.027\ \text{GeV}^{-2}$
$q\bar{q}\gamma\gamma$	a_c^Z	$-0.036\ \text{GeV}^{-2}<a_c^Z/\Lambda^2<0.034\ \text{GeV}^{-2}$
$W^+W^-\gamma$	a_0^W	$-0.020\ \text{GeV}^{-2}<a_0^W/\Lambda^2<0.020\ \text{GeV}^{-2}$
$W^+W^-\gamma$	a_c^W	$-0.053\ \text{GeV}^{-2}<a_c^W/\Lambda^2<0.037\ \text{GeV}^{-2}$

uncertainty. The cross sections for NUNUGPV have been compared with the predictions of Bélanger *et al.* [5] and the difference used to estimate a normalization systematic uncertainty of $\pm 4\%$. In addition, the luminosity error is $\pm 0.3\%$. These errors are added in quadrature to give an estimate of the overall normalization uncertainty of 6.4% which is taken to be independent of energy.

At all center-of-mass energies and for any combination of the couplings, the available NUNUGPV MC statistics amounts to at least one thousand times the data statistics and the related MC statistical error is negligible. Similarly, due to the large sample sizes of random events analyzed, the uncertainties on the corrections for losses due to coincidental random detector hits are less than 1% and are neglected. The systematic error associated with the expected background contribution from processes other than $e^+e^-\to\nu\bar{\nu}\gamma\gamma(\gamma)$ is also negligible.

C. Limits on anomalous QGCs from $e^+e^-\to\nu\bar{\nu}\gamma\gamma$

At each center-of-mass energy, 15 samples of 2 000 events with differing values of a_0^W, a_0^Z, a_c^W and a_c^Z have been simulated. The extra Lagrangian terms are linear in the anomalous couplings. Consequently, the cross section has a quadratic dependence and these 15 samples are sufficient to parametrize fully $\sigma(a_0^W, a_0^Z, a_c^W, a_c^Z)$. The generated events are reweighted using matrix element weights from NUNUGPV to obtain Monte Carlo samples corresponding to any combination of the anomalous QGCs $(a_0^W, a_0^Z, a_c^W, a_c^Z)$.

For the $\nu\bar{\nu}\gamma\gamma$ final state, fits for each of the AQGC parameters have been performed to the data by summing the likelihood curves obtained from the seven center-of-mass energies considered. The effects of systematic uncertainties are included in the fits. The fitted AQGCs are compatible with zero and the resulting 95% confidence level (C.L.) intervals on the anomalous couplings varied individually are listed in Table III. These limits include the effects of systematic uncertainties. The corresponding likelihood curves are shown in Figs. 3(a)–3(d). The results of a fit allowing two AQGC parameters to vary simultaneously are shown in Fig. 4, again with the two parameters not plotted fixed at zero. Since anomalous $ZZ\gamma\gamma$ and $W^+W^-\gamma\gamma$ couplings affect different regions of the invariant mass and second photon energy distributions, the limits on a_0^W and a_0^Z are largely uncorrelated. The same is true for the limits on a_c^W and a_c^Z.

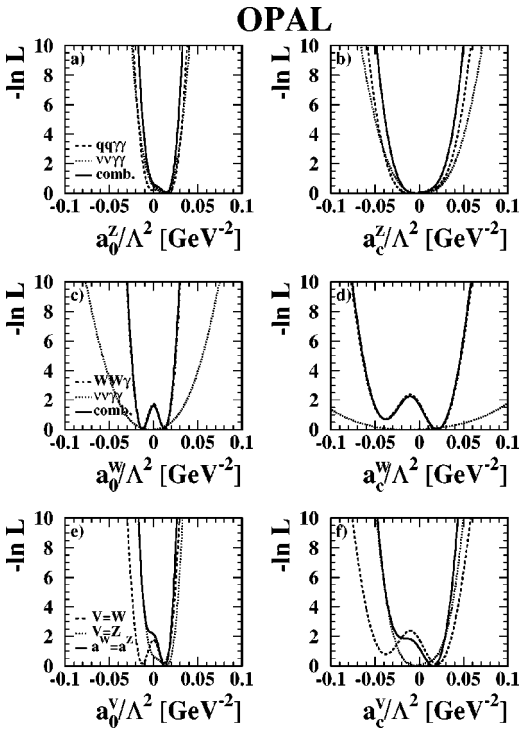

FIG. 3. Plots (a) and (b) show the one dimensional minus log likelihood curves for a_0^Z and a_c^Z from the $\nu\bar{\nu}\gamma\gamma$ channel (dotted line), the $q\bar{q}\gamma\gamma$ channel (dashed line), and the two channels combined (continuous line). Plots (c) and (d) show the one dimensional likelihood curves for a_0^W and a_c^W from the $\nu\bar{\nu}\gamma\gamma$ channel (dotted line), the $W^+W^-\gamma$ channel (dashed line), and the two channels combined (continuous line). Figures (e) and (f) show the combined limits assuming $a_0^Z=a_0^W$ and $a_c^Z=a_c^W$. (e) The one dimensional likelihood curve for $a_0^V=a_0^Z=a_0^W$ (continuous line) with the contribution from the a_0^Z from the $q\bar{q}\gamma\gamma$ and $\nu\bar{\nu}\gamma\gamma$ channels (dotted line) and from the limit on a_0^W from the $W^+W^-\gamma$ and $\nu\bar{\nu}\gamma\gamma$ channels (dashed line). (f) The one dimensional likelihood curve for $a_c^V=a_c^Z=a_c^W$ (continuous line) with the contribution from a_c^Z from the $q\bar{q}\gamma\gamma$ and $\nu\bar{\nu}\gamma\gamma$ channels (dotted line) and from the limit on a_c^W from the $W^+W^-\gamma$ and $\nu\bar{\nu}\gamma\gamma$ channels (dashed line). All likelihood curves include the effects of systematic uncertainties and correspond to the case where only the coupling in question is varied from zero.

V. THE $q\bar{q}\gamma\gamma$ FINAL STATE

In the SM, photons in the process $e^+e^-\to q\bar{q}\gamma\gamma$ are radiated from either the initial or final state fermions. Photons from ISR tend to be produced along the beam direction. Photons from final state radiation (FSR) tend to be produced almost collinear with the quarks and are often lost within

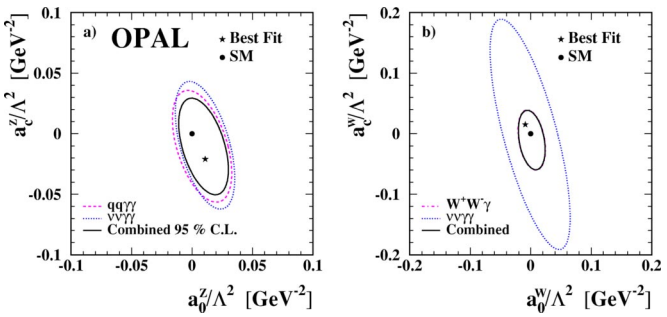

FIG. 4. (a) The 95% confidence region in (a_0^Z, a_c^Z) from the $\nu\bar{\nu}\gamma\gamma$ channel (dotted line), the $q\bar{q}\gamma\gamma$ channel (dashed line), and the two channels combined (continuous line). (b) The 95% confidence region in (a_0^W, a_c^W) from the $\nu\bar{\nu}\gamma\gamma$ channel (dotted line), the $W^+W^-\gamma$ channel [11] (dashed line), and the two channels combined (continuous line). In (b) the limits from the $W^+W^-\gamma$ channel dominate to such an extent that the limits from the $W^+W^-\gamma$ channel alone almost coincide with the combined limit. In both (a) and (b) the position of the best fit (minimum of the $-\ln L$ surface) is indicated by the star and the SM expectation at (0,0) is shown by the point.

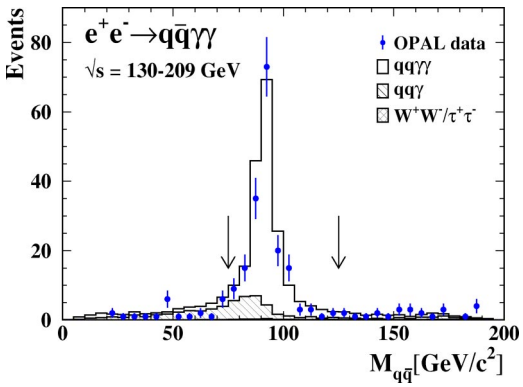

FIG. 5. Invariant mass of the hadronic system, $M_{q\bar{q}}$, in selected $q\bar{q}\gamma\gamma$ events. The arrows indicate the cuts used to select the final $q\bar{q}\gamma\gamma$ sample. The singly hatched histogram indicates the background from $q\bar{q}\gamma$ events and the doubly hatched histogram (barely visible) indicates the small four-fermion and tau-pair backgrounds.

hadronic jets. For the measurement of the $q\bar{q}\gamma\gamma$ cross section a theoretical acceptance is defined which is well matched to the experimental sensitivity. The cross section is defined within a $q\bar{q}$ invariant mass region dominated by the Z exchange diagrams.

The $e^+e^-\to q\bar{q}\gamma\gamma$ cross section measured in this paper corresponds to the following acceptance with respect to the $q\bar{q}\gamma\gamma$ system:

There must be at least two photons satisfying:

(i) $E_{\gamma i}>5$ GeV, where $E_{\gamma i}$ is the energy of photon i,

(ii) $|\cos\theta_{\gamma i}|<0.95$, where $\theta_{\gamma i}$ is the polar angle of photon i,

(iii) $\cos\theta^i_{\gamma q}<0.90$, where $\theta^i_{\gamma q}$ is the angle between photon i and the direction of the nearest quark.

$|M_{q\bar{q}}-M_Z|<3\Gamma_Z$.

The quantity $M_{q\bar{q}}$ is defined as the propagator mass, i.e. the invariant mass of the $q\bar{q}$ system before FSR. Photons from FSR are not considered as signal and interference between ISR and FSR is neglected.

A. $q\bar{q}\gamma\gamma$ event selection

The selection of the $q\bar{q}\gamma\gamma$ events proceeds in three stages:

$e^+e^-\to q\bar{q}$ event selection: $e^+e^-\to q\bar{q}$ events are selected using the algorithm described in [21].

Photon identification: Photon candidates can be identified as either unassociated electromagnetic calorimeter (ECAL) clusters or photon conversions, following the procedure described in [11]. Only photons with measured energy $E_\gamma>5$ GeV and polar angle $|\cos\theta_\gamma|<0.95$ are retained. The remainder of the event is forced into two jets using the Durham algorithm [22]. Finally, to reduce background from photons from the decays of neutral hadrons, e.g. π^0 and η decays, the photons are required to be isolated from the reconstructed jets by requiring $\cos\theta_{\gamma\text{-JET}}<0.9$, where $\theta_{\gamma\text{-JET}}$ is the angle between the photon and the direction of the closest reconstructed jet. Photon candidates which fail this isolation criterion are merged to the nearest jet and the jet energy is recalculated. Events with two or more identified photons satisfying the above requirements are retained for the analysis. For photons within the MC generator level acceptance $E_\gamma>5$ GeV, $|\cos\theta_\gamma|<0.95$ and $\cos\theta_{\gamma q}<0.9$, the photon identification efficiency is about 88%. The requirement of two identified photons therefore rejects approximately 23% of the $q\bar{q}\gamma\gamma$ signal.

Kinematic requirements: The reconstructed mass of the hadronic system, $M_{q\bar{q}}$, is required to be consistent with M_Z. For about 90% of the events $M_{q\bar{q}}$ is obtained from a kinematic fit which imposes the constraints of energy and momentum conservation. In the first instance the fit assumes a four-body final state consisting of two jets and two photons. If the fit probability is less than 0.01, the fit is performed allowing for an unobserved photon along the e^+e^- beam axis. For events where this fit probability is also less than 0.01, the hadronic mass is taken to be the recoil mass calculated from the reconstructed momenta of the two photons. The number of events with mass reconstructed in the three possible categories is consistent with MC expectation. The reconstructed invariant mass spectrum before the cut on $M_{q\bar{q}}$ is shown in Fig. 5. Events within the region 75 GeV$<M_{q\bar{q}}<125$ GeV are considered $q\bar{q}\gamma\gamma$ candidates. The cut on $M_{q\bar{q}}$ removes 47 events in the data compared to the SM expectation of 58.6. Due to experimental resolution this mass window is larger than that used in the kinematic definition of the cross section. Nevertheless, this cut rejects approximately 6% of the $q\bar{q}\gamma\gamma$ events satisfying the signal definition.

After applying the cut on $M_{q\bar{q}}$ a total of 176 events are identified in the data, consistent with the SM expectation of 191.0. Figures 6(a)–6(e) show the distributions of $E_{\gamma 1}$, $E_{\gamma 2}$, $|\cos\theta_{\gamma 1}|$, $|\cos\theta_{\gamma 2}|$ and $E_{\gamma 1}+E_{\gamma 2}$ for selected events. Figure 6(f) shows the distribution of the maximum $|\cos\theta_\gamma|$ of the two highest energy photons in the event. In each case the data are in good agreement with the SM expectation.

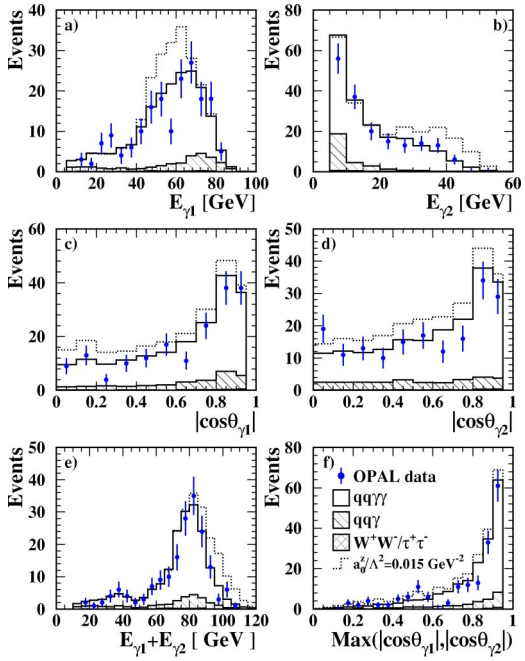

FIG. 6. Distributions of $E_{\gamma 1}$, $E_{\gamma 2}$, $|\cos\theta_{\gamma 1}|$, $|\cos\theta_{\gamma 2}|$, $E_{\gamma 1}+E_{\gamma 2}$ and the maximum of $|\cos\theta_{\gamma 1}|$ and $|\cos\theta_{\gamma 2}|$ for selected $q\bar{q}\gamma\gamma$ events. The points show the 130–209 GeV data and the histograms show the MC expectation. The singly hatched histogram indicates the background from $q\bar{q}\gamma$ events and the doubly hatched histogram indicates the four-fermion and tau-pair backgrounds. The expected distributions for an anomalous QGC parametrized by $a_0^Z/\Lambda^2 = 0.015$ GeV^{-2} are shown by the dotted lines.

B. Cross-section results

The $q\bar{q}\gamma\gamma$ cross section is determined within the above acceptance definition. Cross-section values are obtained for the seven different center-of-mass energy ranges listed in Table IV. The $q\bar{q}\gamma\gamma$ cross section is calculated from

$$\sigma_{q\bar{q}\gamma\gamma} = \frac{(N_{\rm obs} - N_{\rm back}^{\rm MC})}{\varepsilon_{q\bar{q}\gamma\gamma} L},$$

where $N_{\rm obs}$ is the accepted number of events, $N_{\rm back}^{\rm MC}$ is the SM expected number of background events, and $L = \int \mathcal{L} dt$ is the integrated luminosity, given in Table IV. The $q\bar{q}\gamma\gamma$ selection efficiency, $\varepsilon_{q\bar{q}\gamma\gamma}$, is evaluated using the KK2F MC samples and includes feed-through from genuine $q\bar{q}\gamma\gamma$ events outside the signal acceptance (a contribution of approximately 12%).

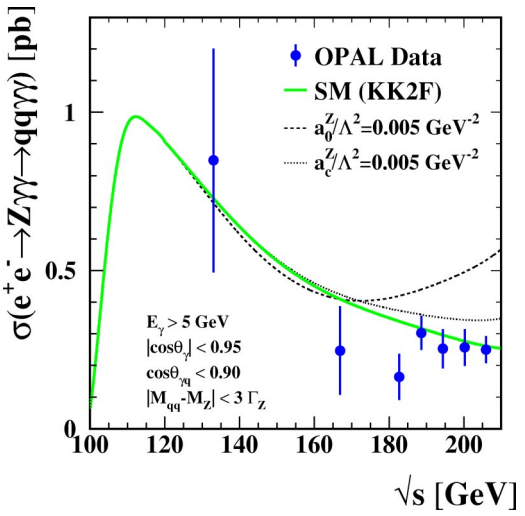

FIG. 7. Measured $e^+e^- \to q\bar{q}\gamma\gamma$ cross-section versus $\sqrt{s}$. The cross section corresponds to the definition given in Sec. V. The SM prediction is obtained from KK2F (without contributions from FSR). The dashed and dotted curves show the effects of anomalous QGCs on the cross section.

The numbers of events selected at each energy are listed in Table IV along with the quantities used to calculate the cross sections. Also shown are the derived cross sections for the above signal acceptance. The systematic uncertainties are described below. The results are consistent with the SM expectation, as shown in Fig. 7. Averaging over all energies, and taking into account correlated systematic uncertainties the ratio of the observed to expected cross sections is

$$R(\text{data/SM}) = 0.92 \pm 0.07 \pm 0.04,$$

where the errors represent the statistical and systematic uncertainties respectively.

TABLE IV. Selected $q\bar{q}\gamma\gamma$ events and cross-section results for the seven different $\sqrt{s}$ ranges used in the analysis. The $\sqrt{s}$ range, the mean luminosity weighted value of $\sqrt{s}$ and the corresponding integrated luminosity, $\int \mathcal{L} dt$, are listed. For the measured cross sections, the uncertainties are respectively statistical and systematic. The uncertainties on the efficiencies and backgrounds are the estimated systematic uncertainties including a contribution from finite MC statistics. Also shown is the SM expectation from KK2F.

$\sqrt{s}$ (GeV)	$\langle\sqrt{s}\rangle$ (GeV)	$\int \mathcal{L} dt$ (pb^{-1})	$\varepsilon_{q\bar{q}\gamma\gamma}$ (%)	$N_{\rm back}^{\rm MC}$	$N_{\rm obs}$	$\sigma_{q\bar{q}\gamma\gamma}$ (fb)	$\sigma_{q\bar{q}\gamma\gamma}$(SM) (fb)
130.0–137.0	133.0	10.6	76.2 ± 4.0	1.1 ± 0.3	8	$848 \pm 350 \pm 57$	738
160.0–173.0	166.9	20.3	79.4 ± 3.2	1.0 ± 0.2	5	$247 \pm 139 \pm 17$	412
180.0–185.0	182.7	57.2	77.5 ± 3.1	2.7 ± 0.5	10	$164 \pm 71 \pm 13$	333
188.0–189.0	188.6	183.1	77.7 ± 2.9	9.5 ± 1.6	53	$305 \pm 51 \pm 16$	309
191.0–196.0	194.4	105.7	77.4 ± 2.9	4.3 ± 0.7	25	$254 \pm 61 \pm 13$	288
199.0–204.0	200.2	114.1	78.4 ± 2.9	3.0 ± 0.6	26	$257 \pm 57 \pm 12$	270
204.0–209.0	205.9	220.6	76.0 ± 2.9	7.2 ± 1.3	49	$250 \pm 47 \pm 12$	257

Systematic uncertainties $(q\bar{q}\gamma\gamma)$

The systematic uncertainties on the $q\bar{q}\gamma\gamma$ selection efficiency and on the expected number of background events are estimated to be 2.7% and approximately 20% respectively. The systematic uncertainties, described below, were obtained in the same manner as described in Ref. [11] where further details may be found. In addition the contributions to the systematic uncertainties due to finite MC statistics are included in the numbers listed in Table IV.

Photon identification and isolation: A systematic uncertainty of 1% is assigned to cover the uncertainties in the simulation of the photon conversion rate and the accuracy of the simulation of the electromagnetic cluster shape [23]. The systematic error associated with the isolation requirements depends on the accuracy of the MC simulation of the fragmentation process in hadronic jets. This is verified in $Z \rightarrow q\bar{q}$ events recorded at $\sqrt{s} \sim M_Z$ during 1998–2000. For each selected event, the inefficiency of the isolation requirements is determined for cones of varying half-angle defined around randomly orientated directions. The inefficiency of the isolation cuts is parametrized as a function of the angle between the cone and the nearest jet. For all cone half-angles the inefficiency in the MC and data agree to better than 1%; consequently a 1% systematic error is assigned. These two effects give a total uncertainty on the identification efficiency for a single photon of 1.4%. Since two photons are required in the analysis of $q\bar{q}\gamma\gamma$ this corresponds to an uncertainty in the $q\bar{q}\gamma\gamma$ efficiency of 2.8%.

Photon energy scale and resolution: A bias in the energy scale for photons (data relative to MC) in the region of the energy cut, i.e. $E_\gamma \sim 5$ GeV, would result in a systematic bias in the $q\bar{q}\gamma\gamma$ cross-section measurement. The uncertainty on the ECAL energy scale for photons in this region is estimated by examining the invariant mass distribution of pairs of photons from π^0 decays in $e^+e^- \rightarrow q\bar{q}$ events recorded at $\sqrt{s} \sim M_Z$ during 1998–2000 and $e^+e^- \rightarrow q\bar{q}(\gamma)$ events recorded at $\sqrt{s} > 180$ GeV. As a result a 4% systematic uncertainty on the ECAL energy scale in the region of $E_\gamma \sim 5$ GeV is assigned. The resulting systematic uncertainty on the $q\bar{q}\gamma\gamma$ cross section is 1.5%.

The systematic error from the uncertainty in the ECAL energy resolution is obtained in a similar manner to that used for the ECAL energy scale using the same π^0 sample. There is no evidence for a statistically significant difference between the energy scales in data and MC. The statistical precision of the comparison, $\pm 10\%$, is used to assign the energy resolution uncertainty which, when propagated to the uncertainty on the $q\bar{q}\gamma\gamma$ cross section, yields a systematic error of $\pm 0.6\%$.

Photon angular acceptance: The systematic error associated with the acceptance requirement of $|\cos\theta_\gamma| < 0.95$ depends on the accuracy of the MC simulation of the angular reconstruction of ECAL clusters at the edge of the acceptance. By comparing the reconstructed polar angle of leptons from different detectors (ECAL, tracking, muon chambers) in $e^+e^- \rightarrow e^+e^-$ and $e^+e^- \rightarrow \mu^+\mu^-$ events the ECAL acceptance is known to ± 3 mrad. This uncertainty results in a 0.6% uncertainty in the $q\bar{q}\gamma\gamma$ cross section.

Background uncertainties (N_{back}^{MC}): The dominant source of background is from $e^+e^- \rightarrow Z/\gamma \rightarrow q\bar{q}\gamma$ where one of the identified photons is from ISR and the other is associated with the hadronic jets. A photon associated with the hadronic jets may be either from FSR in the parton shower or from the decay of a hadron (e.g., π or η decays). From the studies presented in [11] a 30% systematic uncertainty on this background contribution is assumed. The systematic uncertainties on the small background contributions from four-fermion events and from tau-pair events are negligible. An additional 0.8% error is assigned to cover uncertainties in the $e^+e^- \rightarrow q\bar{q}$ selection.

C. Limits on anomalous QGCs from $e^+e^- \rightarrow q\bar{q}\gamma\gamma$

The $e^+e^- \rightarrow q\bar{q}\gamma\gamma$ process is sensitive to the anomalous $ZZ\gamma\gamma$ vertex and the possible couplings a_0^Z, a_c^Z. To set limits on these a binned maximum likelihood fit to the observed distribution of $E_{\gamma 2}$ is performed in 5 GeV bins. Fits are performed to the data for the seven separate energy ranges of Table IV and the resulting likelihood curves are summed. The effects of anomalous couplings are introduced by reweighting events generated with KK2F using the ratio of anomalous QGC to SM matrix elements obtained from the WRAP program [7]. The resulting likelihood curves for one-dimensional fits to a_0^Z and a_c^Z separately are shown in Figs. 3(a) and 3(b). From these curves, 95% C.L. upper limits on the anomalous couplings are obtained, shown in Table III. The limits include the effect of the experimental systematic errors and assume a 5% theoretical uncertainty (obtained by comparing the predictions of KK2F and WRAP over the center-of-mass range considered in this publication). The 95% C.L. contour obtained from a simultaneous fit to a_0^Z and a_c^Z is shown in Fig. 4(a).

VI. COMBINED LIMITS ON ANOMALOUS QGCS FROM THE $q\bar{q}\gamma\gamma$, $\nu\bar{\nu}\gamma\gamma$ AND $W^+W^-\gamma$ PROCESSES

The summed one-dimensional likelihood curves for the parameters a_0^Z and a_c^Z from the $q\bar{q}\gamma\gamma$ and $\nu\bar{\nu}\gamma\gamma$ final states are shown in Figs. 3(a) and 3(b). In this combination the small effect of correlated systematic uncertainties between the two channels has been neglected.[3] The corresponding combined 95% confidence level limits on possible anomalous contributions to the $ZZ\gamma\gamma$ vertex are

$$-0.007 \ \text{GeV}^{-2} < a_0^Z/\Lambda^2 < 0.023 \ \text{GeV}^{-2},$$

$$-0.029 \ \text{GeV}^{-2} < a_c^Z/\Lambda^2 < 0.029 \ \text{GeV}^{-2}.$$

[3]The correlated component of the systematic uncertainty on the event selection efficiencies is estimated to be 2%, dominated by correlated uncertainties from the photon energy scale and photon angular acceptance.

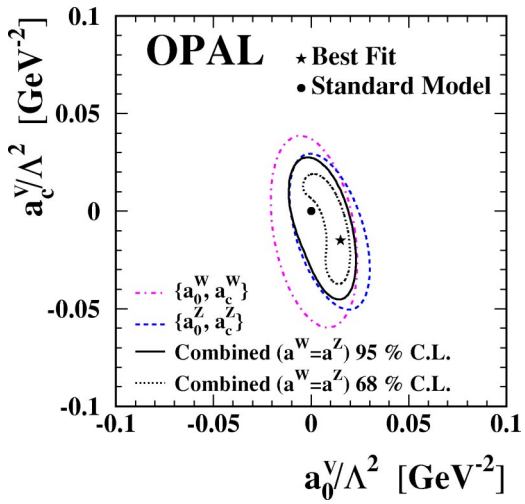

FIG. 8. The 95% confidence region in $(a_0^{\mathrm{V}}, a_c^{\mathrm{V}})$ assuming $a_0^{\mathrm{Z}} = a_0^{\mathrm{W}}$ and $a_c^{\mathrm{Z}} = a_c^{\mathrm{W}}$ (continuous line). Also shown is the 68% confidence region (dotted line). The separate limits on $a_0^{\mathrm{Z}}, a_c^{\mathrm{Z}}$ from the $q\bar{q}\gamma\gamma$ and $\nu\bar{\nu}\gamma\gamma$ channels (dashed line) and from the limits on $a_0^{\mathrm{W}}, a_c^{\mathrm{W}}$ from the $\mathrm{W}^+\mathrm{W}^-\gamma$ and $\nu\bar{\nu}\gamma\gamma$ channels (dot-dashed line) are also shown. The position of the best fit (minimum of the $-\ln \mathrm{L}$ surface) is indicated by the star. The SM expectation at (0,0) is shown by the point.

When both $\mathrm{ZZ}\gamma\gamma$ parameters are allowed to vary simultaneously the likelihood contours of Fig. 4(a) are obtained.

The limits on possible anomalous contributions to the $\mathrm{WW}\gamma\gamma$ vertex obtained here from the $\nu\bar{\nu}\gamma\gamma$ channel are combined with the previous OPAL limits from the $e^+e^- \to \mathrm{W}^+\mathrm{W}^-\gamma$ process [11]. The resulting likelihood curves are shown in Figs. 3(c) and 3(d), again assuming the systematic uncertainties for the two channels are uncorrelated. The double minimum in the likelihood curves is due to a slight excess of $\mathrm{W}^+\mathrm{W}^-\gamma$ events with high energy photons [11]. The corresponding 95% confidence level limits on anomalous contributions to the $\mathrm{W}^+\mathrm{W}^-\gamma\gamma$ vertex are:

$$-0.020 \ \mathrm{GeV}^{-2} < a_0^{\mathrm{W}}/\Lambda^2 < 0.020 \ \mathrm{GeV}^{-2},$$

$$-0.052 \ \mathrm{GeV}^{-2} < a_c^{\mathrm{W}}/\Lambda^2 < 0.037 \ \mathrm{GeV}^{-2}.$$

The likelihood contours for these two parameters are shown in Fig. 4(b).

In the literature the assumption that $a_i^{\mathrm{Z}} = a_i^{\mathrm{W}}$ has been made (see for example Ref. [4]). The validity of the linking of the $\mathrm{W}^+\mathrm{W}^-\gamma\gamma$ and $\mathrm{ZZ}\gamma\gamma$ couplings has been questioned in Ref. [5]. For completeness, limits are presented for the case where $a_i^{\mathrm{Z}} = a_i^{\mathrm{W}}$ by combining the one-dimensional likelihood curves from the $\nu\bar{\nu}\gamma\gamma$, $q\bar{q}\gamma\gamma$ and $\mathrm{W}^+\mathrm{W}^-\gamma$ processes, shown in Figs. 3(e) and 3(f). The combined likelihood yields the 95% confidence level limits:

$$+0.002 \ \mathrm{GeV}^{-2} < a_0^{\mathrm{V}}/\Lambda^2 < 0.019 \ \mathrm{GeV}^{-2},$$

$$-0.022 \ \mathrm{GeV}^{-2} < a_c^{\mathrm{V}}/\Lambda^2 < 0.029 \ \mathrm{GeV}^{-2}.$$

The corresponding two-dimensional fit is shown in Fig. 8.

VII. CONCLUSION

Event selections for the processes $\nu\bar{\nu}\gamma\gamma$ and $q\bar{q}\gamma\gamma$ are presented. The selected $q\bar{q}\gamma\gamma$ events are used to measure the cross section for the process $e^+e^- \to q\bar{q}\gamma\gamma$. Averaging over all energies, the ratio of the observed $e^+e^- \to q\bar{q}\gamma\gamma$ cross section to the standard model expectation is

$$\mathrm{R(data/SM)} = 0.92 \pm 0.07 \pm 0.04,$$

where the errors represent the statistical and systematic uncertainties respectively. The selected $\nu\bar{\nu}\gamma\gamma$ and $q\bar{q}\gamma\gamma$ events are used to constrain possible anomalous $\mathrm{W}^+\mathrm{W}^-\gamma\gamma$ and $\mathrm{ZZ}\gamma\gamma$ couplings. When these results are combined with previous OPAL results from the $\mathrm{W}^+\mathrm{W}^-\gamma$ final state the 95% confidence level limits on the anomalous coupling parameters a_0^{Z}, a_c^{Z}, a_0^{W} and a_c^{W} are found to be:

$$-0.007 \ \mathrm{GeV}^{-2} < a_0^{\mathrm{Z}}/\Lambda^2 < 0.023 \ \mathrm{GeV}^{-2},$$

$$-0.029 \ \mathrm{GeV}^{-2} < a_c^{\mathrm{Z}}/\Lambda^2 < 0.029 \ \mathrm{GeV}^{-2},$$

$$-0.020 \ \mathrm{GeV}^{-2} < a_0^{\mathrm{W}}/\Lambda^2 < 0.020 \ \mathrm{GeV}^{-2},$$

$$-0.052 \ \mathrm{GeV}^{-2} < a_c^{\mathrm{W}}/\Lambda^2 < 0.037 \ \mathrm{GeV}^{-2},$$

where Λ is the energy scale of the new physics. Limits allowing two or more parameters to vary are also presented.

ACKNOWLEDGMENT

We particularly wish to thank the SL Division for the efficient operation of the LEP accelerator at all energies and for their close cooperation with our experimental group. In addition to the support staff at our own institutions we are pleased to acknowledge the Department of Energy, USA, National Science Foundation, USA, Particle Physics and Astronomy Research Council, UK, Natural Sciences and Engineering Research Council, Canada, Israel Science Foundation, administered by the Israel Academy of Science and Humanities, Benoziyo Center for High Energy Physics, Japanese Ministry of Education, Culture, Sports, Science and Technology (MEXT) and a grant under the MEXT International Science Research Program, Japanese Society for the Promotion of Science (JSPS), German Israeli Bi-national Science Foundation (GIF), Bundesministerium für Bildung und Forschung, Germany, National Research Council of Canada, Hungarian Foundation for Scientific Research, OTKA T-038240, and T-042864, and the NWO/NATO Fund for Scientific Research, the Netherlands. E.A.D.W. was supported by Interuniversity Attraction Poles Program–Belgian Science Policy.

[1] G. Bélanger and F. Boudjema, Phys. Lett. B **288**, 201 (1992).
[2] G. Abu Leil and W.J. Stirling, J. Phys. G **21**, 517 (1995).
[3] W.J. Stirling and A. Werthenbach, Phys. Lett. B **466**, 369 (1999).
[4] W.J. Stirling and A. Werthenbach, Eur. Phys. J. C **14**, 103 (2000).
[5] G. Bélanger *et al.*, Eur. Phys. J. C **13**, 283 (2000).
[6] A. Denner, S. Dittmaier, M. Roth, and D. Wackeroth, Eur. Phys. J. C **20**, 201 (2001).
[7] G. Montagna *et al.*, Phys. Lett. B **515**, 197 (2001).
[8] OPAL Collaboration, G. Abbiendi *et al.*, Phys. Lett. B **471**, 293 (1999).
[9] L3 Collaboration, P. Achard *et al.*, Phys. Lett. B **540**, 43 (2001).
[10] L3 Collaboration, P. Achard *et al.*, Phys. Lett. B **527**, 29 (2002).
[11] OPAL Collaboration, G. Abbiendi *et al.*, Phys. Lett. B **580**, 17 (2004).
[12] OPAL Collaboration, K. Ahmet *et al.*, Nucl. Instrum. Methods Phys. Res. A **305**, 275 (1991); OPAL Collaboration, G. Abbiendi *et al.*, Eur. Phys. J. C **14**, 373 (2000); S. Anderson *et al.*, Nucl. Instrum. Methods Phys. Res. A **403**, 326 (1998).
[13] J. Allison *et al.*, Nucl. Instrum. Methods Phys. Res. A **317**, 47 (1992).
[14] G. Montagna, O. Nicrosini, and F. Piccinini, Comput. Phys. Commun. **98**, 206 (1996).
[15] S. Jadach, B.F. Ward, and Z. Wąs, Phys. Lett. B **449**, 97 (1999); S. Jadach, B.F.L. Ward, and Z. Wąs, Comput. Phys. Commun. **130**, 260 (2000).
[16] Program KORALW V1.53 and YFSWW3, S. Jadach *et al.*, Comput. Phys. Commun. **140**, 475 (2001).
[17] Program KORALW V1.42, M. Skrzypek *et al.*, Comput. Phys. Commun. **94**, 216 (1996); M. Skrzypek *et al.*, Phys. Lett. B **372**, 289 (1996); M. Skrzypek *et al.*, Comput. Phys. Commun. **119**, 1 (1999).
[18] T. Sjöstrand, Comput. Phys. Commun. **39**, 374 (1986); T. Sjöstrand and M. Bengtsson, *ibid.* **43**, 367 (1987).
[19] OPAL Collaboration, G. Abbiendi *et al.*, Eur. Phys. J. C **8**, 23 (1999).
[20] OPAL Collaboration, G. Abbiendi *et al.*, Phys. Lett. B **471**, 293 (1999).
[21] OPAL Collaboration, G. Abbiendi *et al.*, Eur. Phys. J. C **33**, 173 (2004).
[22] N. Brown and W.J. Stirling, Phys. Lett. B **252**, 657 (1990); S. Catani *et al.*, *ibid.* **269**, 432 (1991); N. Brown and W.J. Stirling, Z. Phys. C **53**, 629 (1992).
[23] OPAL Collaboration, G. Abbiendi *et al.*, Phys. Lett. B **544**, 29 (2001).